



Effect of CO_2 , HCO_3^- and CO_3^{2-} on oxygen reduction in anion exchange membrane fuel cells

Jose A. Vega, William E. Mustain*

Department of Chemical, Materials and Biomolecular Engineering, University of Connecticut, Storrs, CT 06269, United States

ARTICLE INFO

Article history:

Received 7 August 2009

Received in revised form 14 October 2009

Accepted 17 October 2009

Available online 25 October 2009

Keywords:

Carbon dioxide

Carbonate

Oxygen reduction

Anion exchange membrane

Fuel cell

ABSTRACT

The effect of carbonate and bicarbonate anions on the oxygen reduction reaction was investigated in four alkaline solutions (pH ~ 14) on a Pt disk type electrode with varying concentrations of carbonate and bicarbonate. The addition of carbonate and bicarbonate had two primary effects on the observed voltammetric behavior: i) The Tafel slope shifts positive with increasing carbonate/bicarbonate concentration, indicating that the carbonate anions may compete for surface adsorption sites; and ii) The dissolved oxygen concentration and diffusion coefficient are depressed with increasing anion concentration. Finally, adding CO_2 to the cathode stream of an anion exchange membrane fuel cell caused an improvement in the device performance under fully hydrated conditions, suggesting that the fuel cell was operating at least partially under the carbonate cycle.

© 2009 Elsevier Ltd. All rights reserved.

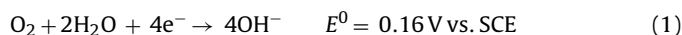
1. Introduction

Anion exchange membrane (AEM) fuel cells are receiving considerable attention due to their advantages over the proton exchange membrane (PEM) fuel cell. First, there are enhanced kinetics for oxygen reduction [1,2] and fuel oxidation reactions [3,4] in the alkaline environment. This allows for the use of non-precious metal electrocatalysts in the cell, which results in a significantly lower cost material than the Pt electrodes required in PEM fuel cells. Also, during operation, anion transport is from cathode to anode and the resulting electroosmotic drag suppresses fuel crossover. The fuel oxidation reaction does not involve water, meaning that alcohol versions can operate on pure fuel, unlike the PEM fuel cell where the fuel must be diluted since water participates in the electrochemical reaction. Recently, there have been several promising reports of hydroxide exchange membrane (HEM) fuel cells using hydrogen, methanol and ethanol as the anode fuel [5–14].

However, the HEM fuel cell still faces some technical limitations. The oxygen reduction reaction (ORR) becomes humidity dependent, which means that the cathode output will vary according to ambient conditions or that water will have to be provided onboard, increasing the complexity of the overall system. Also, the degradation of the electrolyte is catalyzed by hydroxide ions, which causes

two types of degradation: direct nucleophilic displacement and Hoffman elimination [15]. These mechanisms decrease the ionic conductivity by displacing stationary cationic sites responsible for anion transport. This appears to be a difficult hurdle to overcome since the role of the HEM cathode catalyst is to produce hydroxide ions with limited kinetic resistance (high rate) and the role of the electrolyte is to transport those ions efficiently.

Over the past few decades, there have been several studies regarding the impurity tolerance of liquid electrolyte alkaline fuel cells (AFCs) [16,17]. One of the most cumbersome impurities in the AFC is CO_2 which has shown to cause significant performance degradation when the AFC is operated in air [18], where the following reactions proceed:



Here, Eq. (1) is the typical four electron oxygen reduction in alkaline media. Eqs. (2) and (3) represent thermodynamic equilibrium between hydroxide, bicarbonate and carbonate ions in aqueous media. The carbonate and bicarbonate ions react with the potassium cations in the aqueous electrolyte forming KHCO_3 and K_2CO_3 salts, which have low solubility in aqueous environments. These salts accumulate on the electrodes, diminishing their performance and eventually rendering the fuel cell completely inactive.

However, it is still unclear what effect CO_2 will have in the AEM fuel cell. It is well known that in order to conduct ions the membrane must be humidified. When CO_2 is dissolved in water it can

* Corresponding author at: Department of Chemical, Materials and Biomolecular Engineering, University of Connecticut, Unit 3222, 191 Auditorium Rd, Storrs, CT 06269, United States. Tel.: +1 860 486 2756; fax: +1 860 486 2959.

E-mail address: mustain@enr.uconn.edu (W.E. Mustain).

from carbonic acid (Eq. (4)) which can later form carbonate ions in the alkaline environment of the fuel cell (Eq. (5)):



The presence of carbonate ions could diminish the conductivity of the electrolyte mostly because the larger size of this anion compared to hydroxide. Carbonate ions will also lower the local pH in the electrodes and electrolyte, and it is unclear the effect this could have on the anode and cathode kinetics. The ORR has been previously studied in dilute and concentrated alkaline aqueous conditions [19], as well as in carbonate-only aqueous solutions [20]. However the effect of both carbonate and bicarbonate on the ORR in highly alkaline environments has not been reported.

The purpose of this study is to elucidate the effect of carbonate/bicarbonate on the ORR in alkaline electrolytes. This was done by studying oxygen reduction with a platinum electrode in electrolytes containing 1 M KOH and varying concentrations of sodium carbonate and sodium bicarbonate. Physical properties of the electrolytes were determined and kinetic and mass transfer analysis was performed using Koutecky–Levich and Tafel plots. The performance of a full AEM fuel cell was also investigated in the presence of different concentrations of CO_2 in the cathode stream.

2. Experimental

A polycrystalline platinum disk/Pt ring rotating ring-disk electrode (RRDE) was used as the working electrode in this study to explore the oxygen reduction kinetics. A platinum foil, several times larger than the working electrode, was used as the counter electrode. A saturated calomel electrode (SCE) was used as the reference electrode and all potentials are reported relative to the SCE. Prior to experimentation, the 0.196 cm² Pt-disk was polished to a 0.05 μm finish, thoroughly rinsed with 18 MΩ Millipore water and fresh electrolyte solution and electrochemically cycled twenty times at 50 mV/s between –1.05 and 0.2 V to ensure a clean and active surface. The reference and counter electrodes were also rinsed with Millipore water and fresh electrolyte prior to experimentation. The electrodes were inserted in a three compartment jacketed glass cell with a Luggin capillary for the reference electrode compartment and the counter electrode compartment separated from the cell by an ionic conducting, fritted glass separator.

KOH, Na₂CO₃ and NaHCO₃ (ACS reagent grade) were dissolved in 18 MΩ Millipore water to make solutions of the following concentrations: 1 M KOH; 1 M KOH & 0.01 M Na₂CO₃/NaHCO₃; 1 M KOH & 0.05 M Na₂CO₃/NaHCO₃; 1 M KOH & 0.1 M Na₂CO₃/NaHCO₃. Viscosities were obtained using a size 25 Cannon-Fenske Routine viscometer (Cannon Instruments). pH and dissolved oxygen (DO) concentration were measured with an Accumet Excel XL 60 pH and DO meter. Before each experiment, the electrolyte was bubbled with argon for 1 h followed by 1 h of oxygen bubbling to ensure O₂ saturation. All experiments were thermostated at a solution temperature of 25 ± 0.1 °C. The polarization curves were obtained with

an Autolab PGSTAT302N potentiostat. The RRDE rotation speed was controlled with an AFMSRCE analytical rotator (Pine Instrument Company).

Fuel cell experiments were carried out with an 850e Fuel Cell Test Station from Scribner Associates Inc. Humidified hydrogen was used as the anode gas, while humidified oxygen, carbon dioxide and nitrogen were used as cathode gas; all gases were obtained from Airgas. Experiments were carried out at a cell temperature of 30 °C. Membrane-electrode assemblies were prepared using a Ralex AMH-PAD anion exchange membrane (Mega a.s.). The membrane anion was exchanged from chloride to carbonate by soaking the membrane in a 1 M Na₂CO₃ solution for 24 h with one change of solution in between. A catalyst ink was made from platinum supported on carbon (10%Pt/C) suspended in dimethylformamide (DMF) and painted on 5 cm² carbon paper to a total catalyst loading of 4 mg/cm². The membrane-electrode assembly (MEA) was loaded in the fuel cell hardware and humidified overnight before experimentation.

3. Results and discussion

3.1. Electrolyte characterization

The alkaline electrolytes under study were prepared from 1 M KOH solutions and further addition of various quantities of carbonate/bicarbonate. Sodium carbonate and sodium bicarbonate were added in equal quantities to obtain solutions containing 0.01 M, 0.05 M and 0.1 M of both CO₃²⁻ and HCO₃⁻ anions. Several physical properties of interest (kinematic viscosity, density, dissolved oxygen concentration, oxygen diffusion coefficient) were determined through experiments or calculations and are shown in Table 1 (A, 1 M KOH; B, 1 M KOH and 0.01 M Na₂CO₃/NaHCO₃; C, 1 M KOH and 0.05 M Na₂CO₃/NaHCO₃; D, 1 M KOH and 0.1 M Na₂CO₃/NaHCO₃).

The kinematic viscosity, ν , was measured with a glass viscometer immersed in a water bath thermostated at 25 ± 0.2 °C. The viscometer was kept in the water bath for 30 min prior to experimentation to ensure thermal equilibrium of the system. Three measurements were taken and the average value is reported; however, the difference in the measurements taken for one given solution was less than 1%. The solution density, ρ , was obtained by measuring 1 mL of the solution with a micropipette and determining its mass with a P-114 analytical balance (Denver Instruments). Three measurements were taken; the average value is reported, though differences in measurements were less than 2%. Then, the solution viscosity was obtained by Eq. (6):

$$\mu = \nu \times \rho \quad (6)$$

Oxygen diffusion coefficients were estimated by the Hayduk–Laudie correlation [21] (Eq. (7)), which applies for nonelectrolytes in water,

$$D_{AB}^0 = \frac{13.26 \times 10^{-9}}{\mu_B^{1.14} \nu_A^{0.589}} \quad (7)$$

Table 1

Physical properties of (A) 1 M KOH, (B) 1 M KOH, 0.01 M Na₂CO₃, 0.01 M NaHCO₃, (C) 1 M KOH, 0.05 M Na₂CO₃, 0.05 M NaHCO₃ and (D) 1 M KOH, 0.1 M Na₂CO₃, 0.1 M NaHCO₃.

| Solution | ν^a (cSt) | ρ^b (g mL ⁻¹) | μ^c (cP) | $D^d \times 10^5$ (cm ² s ⁻¹) | C _{oxygen} (mM) | pH |
|----------|---------------|--------------------------------|--------------|--|--------------------------|-------|
| A | 0.93 | 1.04 | 0.97 | 2.04 | 0.86 | 14.30 |
| B | 0.93 | 1.04 | 0.97 | 2.04 | 0.86 | 14.28 |
| C | 0.96 | 1.05 | 1.01 | 1.94 | 0.81 | 14.24 |
| D | 1.0 | 1.06 | 1.06 | 1.83 | 0.76 | 14.18 |

^a Kinematic viscosity.

^b Density.

^c Viscosity.

^d Oxygen diffusion coefficient.

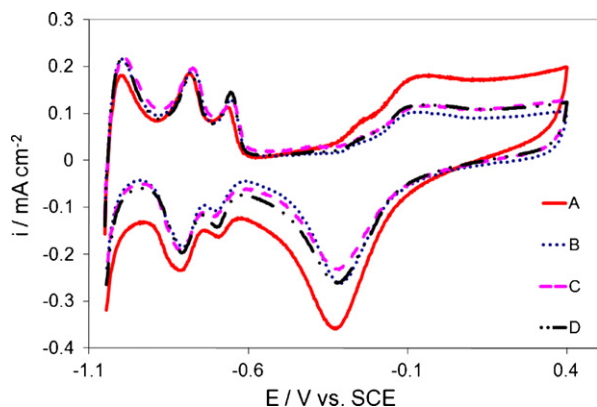


Fig. 1. Cyclic voltammogram at 100 mV/s and 25 °C for a polycrystalline Pt-disk electrode in Ar-purged (A) 1 M KOH, (B) 1 M KOH, 0.01 M Na₂CO₃, 0.01 M NaHCO₃, (C) 1 M KOH, 0.05 M Na₂CO₃, 0.05 M NaHCO₃ and (D) 1 M KOH, 0.1 M Na₂CO₃, 0.1 M NaHCO₃.

where μ is the solvent viscosity in cP and V_A is the molar volume of the liquid solute at its normal boiling point in cm³/mol, taken as 25.6 cm³/mol. The 1.14 exponential in the viscosity compensates for the absence of an explicit temperature dependence. The equation has a maximum error of 5.9% [5]. The DO concentration was determined after bubbling oxygen gas through the electrolyte for 1 h to ensure saturation. Steady oxygen flow was maintained in the headspace of the cell during measurement to yield an oxygen only atmosphere and the temperature was controlled at 25 ± 0.2 °C. Oxygen saturation concentration values for 1 M KOH found in the literature [22] closely resemble the value shown in Table 1.

3.2. Cyclic voltammetry

Typical cyclic voltammograms (CVs) for a polycrystalline platinum electrode in Argon purged electrolytes at 100 mV/s were obtained and are shown in Fig. 1. The positions of the hydrogen peaks are at the potentials expected for a solution with pH ~ 14 and correspond to the adsorption and reaction of H₂, hydroxide and water. No considerable difference is seen in peak potential since addition of carbonate/bicarbonate results in minimal changes in pH (Table 1). The double layer region is wider when no carbonate/bicarbonate is present in the solution and platinum oxidation and reduction is considerably larger. This is consistent with the literature [20] as substitution of hydroxide ions in solution with carbonate ions has shown a decrease in double layer thickness due to the increase in ionic strength of the electrolyte. This is also consistent with the Debye length, which describes the thickness of the electrical double layer and predicts a decrease in the double layer thickness as the concentration of ions or their valence increase [23]. Also, the 1 M KOH solution produces a higher amount of surface oxides during the cathodic scan, leading to increased oxygen evolution during the anodic scan shifting the curve negative; therefore the change in double layer capacitance appears not to be equidistant in the cathodic and anodic portions of the scan.

Saturation of the electrolytes with O₂ causes a considerable increase in the oxygen reduction current (Fig. 2), compared to the Ar-purged electrolytes, with no considerable difference in the platinum oxidation, as expected. The double layer increases due to the presence of oxygen and, consequentially, the increase in oxygen exchange current. However, the amount of platinum oxides formed for the carbonate/bicarbonate containing solutions appears to be the same. The oxygen reduction current decreases with higher contents of salt. This is expected considering that the oxygen concentration and diffusion coefficient diminish with increased salt concentration. This is also indicated by the reduced magnitude

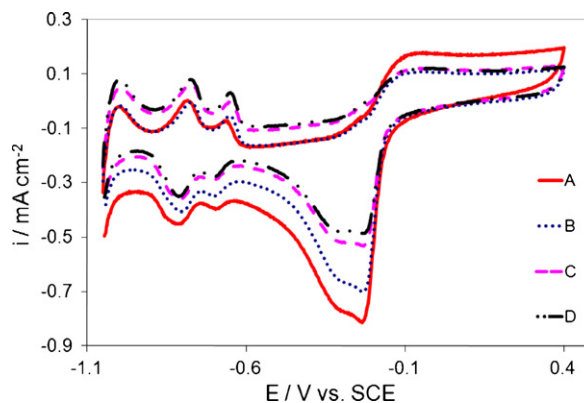


Fig. 2. Cyclic voltammogram at 100 mV/s and 25 °C for a polycrystalline Pt-disk electrode in O₂-purged (A) 1 M KOH, (B) 1 M KOH, 0.01 M Na₂CO₃, 0.01 M NaHCO₃, (C) 1 M KOH, 0.05 M Na₂CO₃, 0.05 M NaHCO₃ and (D) 1 M KOH, 0.1 M Na₂CO₃, 0.1 M NaHCO₃.

of the current shift in the hydrogen region (between -0.6 and -1 V) with increased carbonate/bicarbonate concentration. Lastly, addition of 0.01 M carbonate/bicarbonate does not cause any appreciable changes in the electrolyte physical properties, though a decrease in the oxygen reduction current is observed. This suggests a possible change in the active electrode area or the number of electrons for the reaction, two additional factors that could affect the current magnitude considering the scan rate is constant. Calculation of the charge in the hydrogen adsorption region from Fig. 1, subtracting the double layer contribution, was 7.1 mC on average for all solutions. Deviation from this value did not exceed 2.5% on any electrolyte, which suggests negligible changes in the electrode active area with addition of carbonate/bicarbonate.

3.3. Oxygen reduction

The oxygen reduction proceeds through two main pathways: a direct four electron reduction to hydroxide and a two electron reduction to hydrogen peroxide. The two electron transfer process can possibly involve another two electron process that converts the hydrogen peroxide to OH⁻. Data obtained from ring-disk measurements can serve to distinguish between the pathways for O₂ reduction. The simplified scheme for oxygen reduction in alkaline solution is shown in Fig. 3 [24].

Linear sweep voltammograms in O₂-saturated electrolytes were obtained at four rotation rates (400, 900, 1600 and 2500 RPM) with a 1 mV/s scanrate on the Pt-disk. The Pt ring, held at a potential of 0.3 V vs. SCE, was used to confirm the production of hydrogen peroxide during oxygen reduction.

For a rotating disk electrode experiment the observed current is expressed by

$$\frac{1}{i} = \frac{1}{i_k} + \frac{1}{i_L} = \frac{1}{i_k} + \frac{1}{B\omega^{1/2}} \quad (8)$$

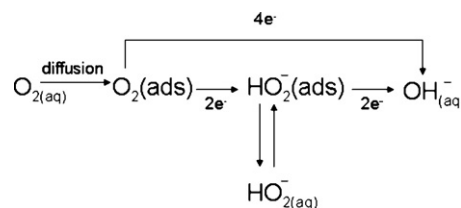


Fig. 3. Simplified mechanism for the electrochemical reduction of molecular oxygen in alkaline solution.

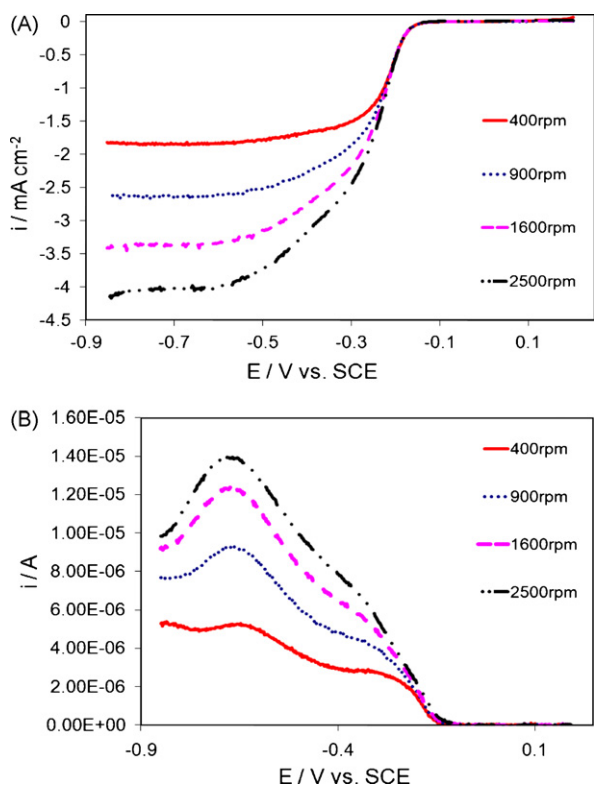


Fig. 4. Cathodic voltammograms for (A) Pt-disk and (B) Pt ring in O_2 -saturated 1 M KOH at 1 mV/s and 25 °C.

where i is the observed current, i_k is the kinetic current and i_L is the mass transport limited current. Mass transport limited currents for a rotating disk electrode are described by the Levich equation:

$$i_L = 0.62nFAD_0^{2/3}\omega^{1/2}\nu^{-1/6}C_0 = B\omega^{1/2} \quad (9)$$

where n is the overall number of electrons transferred during reaction, F is the Faraday constant, A is the electrode active area, D is the oxygen diffusion coefficient, ω is the rotation rate, ν is the kinematic viscosity and C is the dissolved oxygen concentration. B is expressed by

$$B = 0.62nFAD_0^{2/3}\nu^{-1/6}C_0 \quad (10)$$

Cathodic voltammograms (−0.85 to 0.2 V vs. SCE) for the Pt-disk at various rotation rates for oxygen saturated 1 M KOH are shown in Fig. 4a. Fig. 4a shows that the mass transport controlled currents are proportional to the square root of the rotation rate, as described by Eq. (9). Fig. 4b shows cathodic voltammograms for the Pt ring in the same solution. The ring current, corresponding to the diffusion controlled oxidation of hydrogen peroxide, shows some complex behavior. There are peaks and a maximum present, consistent with the literature [20,25,26]. In this study, peaks are located at potentials of approximately −0.3 and −0.67 V, with the current reaching a maximum at −0.67 V. At 400 RPM, the maximum is not clearly visible, but the peak at −0.3 V is more defined than at other rotation rates. The ring current is over one order of magnitude lower than the disk current (after correction for collection efficiency $N = 25.1\%$), which confirms that the principal reaction at the disk electrode is the complete four electron oxygen reduction to hydroxide.

Linear sweep voltammograms for the Pt RDE at 400 RPM in all the O_2 -saturated electrolytes are shown in Fig. 5. The region with mixed kinetic and diffusion control (approximately −0.2 to −0.35 V) shows its highest current when the carbonate/bicarbonate concentration is 0 M, followed by 0.05 M, 0.1 M and finally 0.01 M. The onset potential for oxygen reduction follows the

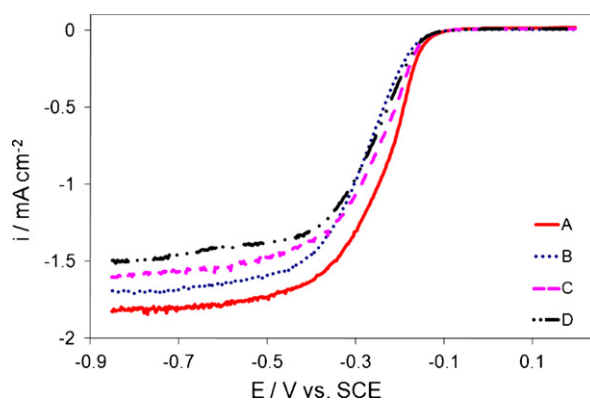


Fig. 5. Cathodic voltammograms for Pt-disk in O_2 -saturated (A) 1 M KOH, (B) 1 M KOH, 0.01 M Na_2CO_3 , 0.01 M $NaHCO_3$, (C) 1 M KOH, 0.05 M Na_2CO_3 , 0.05 M $NaHCO_3$ and (D) 1 M KOH, 0.1 M Na_2CO_3 , 0.1 M $NaHCO_3$ at 1 mV/s and 25 °C.

same pattern, becoming more negative with the first addition of carbonate/bicarbonate and subsequently becoming more positive, although overall the difference in onset potential is relatively small.

In the diffusion limited region, the current continuously decreases as the amount of carbonate/bicarbonate increases in the electrolyte. This is expected, according to Eq. (9), since oxygen concentration and diffusion coefficient decrease and kinematic viscosity increases when more salt is present in solution (Table 1). This is consistent with the observation of lower oxidation currents with higher contents of salt in Figs. 1 and 2.

To provide a balanced comparison between the RRDE disk plots, it is useful to normalize the observed current to the oxygen diffusion coefficient, electrolyte kinematic viscosity and the oxygen saturation concentration, which can be done using Eq. (11):

$$i_{normalized} = \frac{i_{observed}}{D_0^{2/3}\nu^{-1/6}C_0} = 0.62nFA \quad (11)$$

After normalization, the diffusion limited current depends only on the number of electrons in the reaction and the electrode active area. The mass transport region of a graph of $i_{normalized}$ vs. potential should overlay if these two parameters do not change with electrolyte composition.

Fig. 6 shows cathodic voltammograms of the normalized current on a Pt-disk for all electrolytes at 400 RPM. Although normalization was performed for the complete potential range, the mass transport limited region of the voltammogram provides the information since normalization is done with mass transport parameters. The mixed control region shows the same trend in current magnitudes

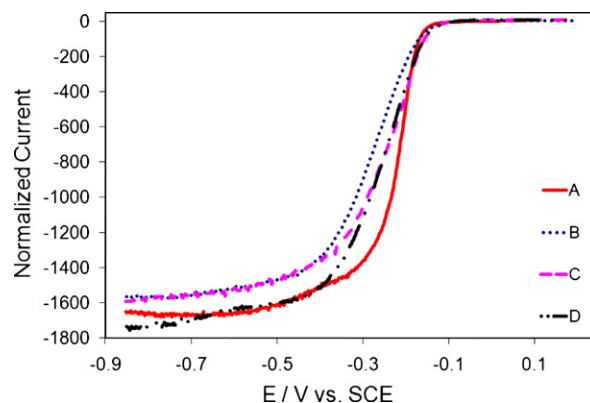


Fig. 6. Linear sweep voltammograms showing normalized currents for Pt-disk in O_2 -saturated (A) 1 M KOH, (B) 1 M KOH, 0.01 M Na_2CO_3 , 0.01 M $NaHCO_3$, (C) 1 M KOH, 0.05 M Na_2CO_3 , 0.05 M $NaHCO_3$ and (D) 1 M KOH, 0.1 M Na_2CO_3 , 0.1 M $NaHCO_3$.

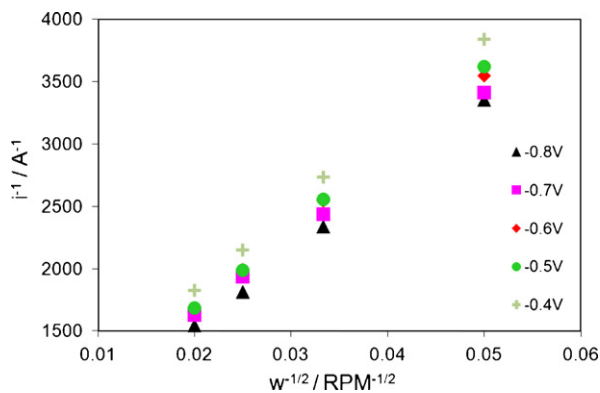


Fig. 7. Koutecky–Levich plot for ORR at various potentials in the 1 M KOH and 0.1 M $\text{Na}_2\text{CO}_3/\text{NaHCO}_3$ electrolyte.

as Fig. 5 for all electrolytes. Clearly, there are differences in the normalized current of the mass transport region. For electrolytes A, B and C the normalized current does not vary by over 3% indicating that carbonate/bicarbonate does not have a pronounced effect on n or the electrode active area. However, electrolyte D shows a larger difference of approximately 10%. This difference is statistically significant considering that the diffusion coefficient equation, with an accuracy of 5.9%, introduces only a 4% error in estimating i_L . There is also the error related to the measurement of the other properties, although these are, as mentioned previously, minimal. However, the normalized voltammogram of electrolyte D does not follow the same general shape as the other electrolytes. The absolute value of the normalized current for electrolyte D continuously increases, contrary to the other electrolytes in which the normalized current appears to reach a true limiting value. It appears that the introduction of carbonate and bicarbonate affects the current magnitude at higher ionic concentrations (electrolyte D), while the addition of smaller quantities (electrolytes B and C) has a minimal effect. However, the effect of addition of high concentrations of carbonate/bicarbonate ions should be studied in more detail to confirm its effect.

Koutecky–Levich plots of $1/i$ vs. $1/\sqrt{\omega}$ at various potentials should yield straight lines with the intercept corresponding to $1/i_k$ and the slope yielding $1/B$. Such plots are shown in Fig. 7 for the cathodic scan of the 1 M KOH and 0.1 M $\text{Na}_2\text{CO}_3/\text{NaHCO}_3$ electrolyte. Here, straight lines are obtained and the slope remains nearly constant over the potential range -0.8 to -0.4 V. The number of electrons transferred can be obtained from the B value and Eq. (10), since physical properties are known (Table 1), and the electrode active area is assumed to equal the total electrode area. Table 2 shows values of $n=3.8$ for the 1 M KOH and $n=3.9$ for all other electrolytes at -0.7 V, with n remaining constant throughout the mass transfer limited region. This indicates that over 95% of the dissolved oxygen reacts through the four electron pathway forming water and a minimal quantity undergoes the two electron reduction to hydrogen peroxide. This is consistent with the observed ring current in all electrolytes, which was always more than an order

Table 2

Parameters obtained from Koutecky–Levich and Tafel plots for (A) 1 M KOH, (B) 1 M KOH, 0.01 M Na_2CO_3 , 0.01 M NaHCO_3 , (C) 1 M KOH, 0.05 M Na_2CO_3 , 0.05 M NaHCO_3 and (D) 1 M KOH, 0.1 M Na_2CO_3 , 0.1 M NaHCO_3 .

| Solution | $1/B^a$ | n^a | Tafel slope (mV decade^{-1}) |
|----------|---------|-------|---|
| A | 16,109 | 3.8 | 120 |
| B | 15,167 | 3.9 | 130 |
| C | 17,106 | 3.9 | 134 |
| D | 19,216 | 3.9 | 139 |

^a Potential = -0.7 V.

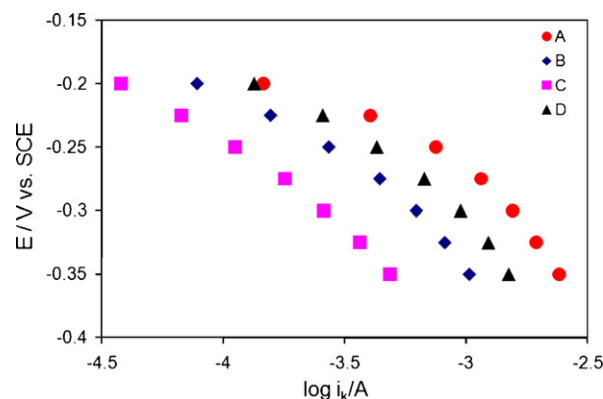


Fig. 8. Tafel plots for O_2 -saturated (A) 1 M KOH, (B) 1 M KOH, 0.01 M Na_2CO_3 , 0.01 M NaHCO_3 , (C) 1 M KOH, 0.05 M Na_2CO_3 , 0.05 M NaHCO_3 and (D) 1 M KOH, 0.1 M Na_2CO_3 , 0.1 M NaHCO_3 .

of magnitude lower than the disk current, after correction for the collection efficiency.

Tafel plots ($\log i_k$ vs. E) for the cathodic scans are shown in Fig. 8 for all electrolytes. Kinetic currents were obtained from the intercept of the Koutecky–Levich plots in Fig. 7. The magnitude of the kinetic current is highest with a 0 M concentration of carbonate/bicarbonate, followed by 0.1 M, 0.01 M and finally 0.05 M. The pattern is different than for the observed current in the mixed kinetic-mass transfer region. For example, electrolyte C has the lowest magnitude kinetic current although it had the second highest observed current in the mixed region; therefore mass transfer makes a significant contribution in the total current of this electrolyte in the -0.2 to -0.35 V region. In general, the magnitude of the kinetic current in the mixed control region does not follow the same pattern as the magnitude of the mass transfer current. A decrease in kinetic current with addition of carbonate and bicarbonate ions could indicate a slight competition for ion adsorption between OH^- , HCO_3^- and CO_3^{2-} , which would resemble what was observed in the mass transport limited region. However, the reason for an increase in kinetic current with 0.1 M carbonate/bicarbonate is not clear; again, it appears that larger additions of carbonate and bicarbonate have a considerable effect on oxygen reduction. However, alkaline electrolytes containing only carbonate have been demonstrated to provide higher kinetic current, at least after normalization to the dissolved oxygen concentration [20].

The Tafel slope obtained from Fig. 8 for all the electrolytes is reported in Table 2. The 1 M KOH electrolyte has a Tafel slope of 120 mV/decade which suggest that the initial electron transfer is the rate determining step. The Tafel slope gradually increases as the amount of carbonate/bicarbonate in solution increases (Table 2), however the slope magnitude suggests the initial electron transfer is still the rate determining step.

The difference in the Tafel slope could be related to the behavior observed in Fig. 6. The slight change in the normalized current could indicate carbonate/bicarbonate adsorption on the electrode surface therefore affecting the active area and the rate of oxygen reduction. Coverage of the electrode area by an inactive species can affect the one-site or two-site adsorption of oxygen. This would cause a shift in the possible pathways for oxygen reduction, resulting in a mildly altered Tafel slope.

3.4. Anion exchange membrane fuel cell

In this work, the Ralex AMH-PAD anion exchange membrane was converted to the carbonate form and different ratios of oxygen to carbon dioxide were used to observe the effect CO_2 has on fuel cell performance. The carbonate form AEM fuel cell has

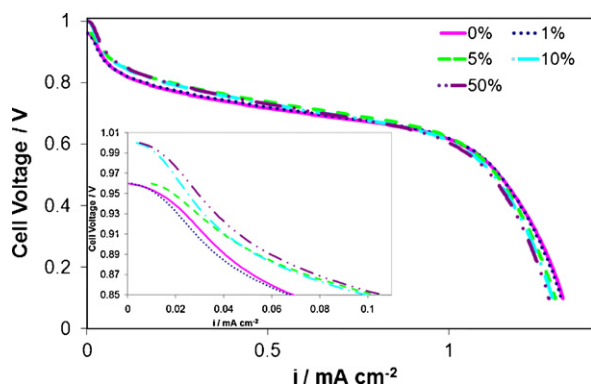


Fig. 9. Polarization curves for AEM fuel cell with different CO₂ content in the cathode stream at 50 mV/s.

been shown to provide an increase in the power density compared to the hydroxide form, which was attributed to the higher ion exchange capacity or higher valence of the carbonate ion compared to hydroxide [27]. Membranes with the carbonate anion have also been shown to maintain their conductivity for a longer period of time than membranes with the hydroxide anion [28].

Fig. 9 shows linear sweep polarization curves for the AEM fuel cell between the open circuit voltage (OCV) and 0.1 V at a scan rate of 50 mV/s. The OCV increased slightly as additional CO₂ was added to the cathode stream. The inset in Fig. 9 shows the kinetic region of the scan. In the kinetic region, the current diminishes when 1% CO₂ is mixed with the oxygen. However, there is an increase in current when more CO₂ is added to the cathode stream. This behavior resembles that observed in solution-phase experiments (Fig. 5) where an initial addition of a small quantity of carbonate/bicarbonate caused a decrease in current in the mixed region, but further additions of salt caused an improvement in the current. This could be explained by the higher kinetic current observed in carbonate-only solutions, after normalization for oxygen concentration, compared with hydroxide only solutions [20]. The mass transfer region shows a small continuous decrease in current as more CO₂ is present in the cathode stream. This also resembles the behavior observed in solution (Fig. 5) where continuous addition of carbonate/bicarbonate caused a decrease in the mass transfer limited current.

When carbon dioxide was replaced by nitrogen gas, a clear difference was observed in the kinetic region (Fig. 10) compared with CO₂ (Fig. 9). The current continuously decreased as more nitrogen was added, since the oxygen concentration is being diminished and reaction sites in contact with nitrogen do not participate in the reactions. The mass transport limited region also shows a contin-

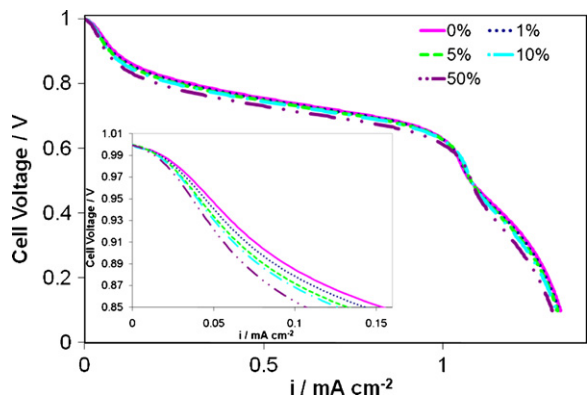
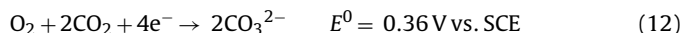


Fig. 10. Polarization curves for AEM fuel cell with different N₂ content in the cathode stream at 50 mV/s.

uous decrease as N₂ increases. The difference in the kinetic region between Figs. 9 and 10 shows that CO₂ does not merely act as an inert diluent, like N₂; it is actually involved in the reaction. So, not only is the oxygen reduction reaction in the AEM fuel cell CO₂ and carbonate tolerant, it appears that the AEM fuel cell is operating at least partially on the carbonate cycle. This is consistent with the work by the Kohl group, which have demonstrated AEM fuel cells operating on the carbonate cycle with carbon supported Pt catalyst at both the anode and cathode [28,29]. However it remains unclear if the carbonate route proceeds through the direct (Eq. (12)) or the hydroxide pathway (Eqs. (1)–(3)):



This work, combined with references 28, 29 and 30, suggest that the carbonate cycle represents a promising alternative to the traditional hydroxide AEM fuel cell. Not only is the oxygen reduction assisted by carbonate ions, the carbonate ion provides a lower localized pH than hydroxide, which may significantly improve electrolyte durability. This will allow use of already developed low-cost anion exchange membranes.

However, there are still issues to overcome for improved operation of an AEM fuel cell on the carbonate cycle. Most notably, the selective formation of carbonate over hydroxide at the cathode, since hydroxide formation is preferred on platinum catalysts under humidified conditions. Also, it is still unclear what effect the carbonate anions will have on H₂ oxidation in the AEM fuel cell. Therefore the development of catalyst for the selective adsorption of O₂ and CO₂ and reduction to carbonate anions is an area of significant potential improvement. The use of an anion exchange ionomer in the catalyst ink will improve the membrane-electrode electrical contact which will result in significantly higher current densities.

4. Conclusions

The effect of carbonate on the ORR was investigated in alkaline solutions and alkaline fuel cells. Carbonate ions have a small effect on the ORR in alkaline environments. After considering several physical properties, the minimal effect appears to be due to carbonate adsorption on the electrode, which slightly reduces the active area, affecting oxygen adsorption and the reaction kinetics. Adding CO₂ to an AEM fuel cell has no deleterious effect on the cell performance. In fact, an improvement in the fuel cell performance in the kinetic region current was observed with addition of CO₂ to the cathode stream. Comparison with the use of N₂, instead of CO₂, suggested the fuel cell was operating through the carbonate cycle. Therefore, there is promise to operate on the carbonate cycle at low temperatures, which would give a local decrease in pH, improving the electrolyte durability. However, much work remains to find carbonate selective catalysts under fully hydrated cell conditions.

References

- [1] N. Markovic, H. Gasteiger, P. Ross, J. Phys. Chem. 100 (1996) 6715.
- [2] L. Demarconay, C. Coutanceau, J. Leger, Electrochim. Acta 49 (2004) 4513.
- [3] Y. Kuros, S. Schwartz, J. Power Sources 87 (2000) 101.
- [4] J. Hernandez, J. Solla-Gullon, E. Herrero, A. Aldaz, J. Feliu, Electrochim. Acta 52 (2006) 1662.
- [5] G. Hebrard, J. Zeng, K. Loubiere, Chem. Eng. J. 148 (2009) 132.
- [6] J. Park, et al., J. Power Sources 178 (2008) 620.
- [7] E. Agel, J. Bouet, J. Fauvarque, J. Power Sources 101 (2001) 267.
- [8] E. Yu, K. Scott, Electrochem. Commun. 6 (2004) 361.
- [9] L. Li, Y. Wang, J. Membr. Sci. 262 (2005) 1.
- [10] H. Hou, G. Sun, R. He, Z. Wu, B. Sun, J. Power Sources 182 (2008) 95.
- [11] J. Varcoe, R. Slade, E. Yee, Chem. Commun. 13 (2006) 1428.
- [12] Y. Wu, C. Wu, F. Yu, T. Xu, Y. Fu, J. Membr. Sci. 307 (2008) 28.
- [13] Y. Xiong, J. Fang, Q. Zeng, Q. Liu, J. Membr. Sci. 311 (2008) 319.
- [14] E. Yu, K. Scott, J. Power Sources 137 (2004) 248.
- [15] J. Varcoe, R. Slade, Fuel Cells 5 (2005) 187.
- [16] M. Alsaleh, S. Gultekin, A. Alzakri, H. Celiker, J. Appl. Electrochem. 24 (1994) 575.

- [17] S. Gultekin, M. Alsaleh, A. Alzakri, *Int. J. Hydrogen Energy* 19 (1994) 181.
- [18] A. Tewari, V. Sambhy, M. Urquidi Macdonald, A. Sen, *J. Power Sources* 153 (2006) 1.
- [19] C. Zhang, F.-R. Fan, A. Bard, *J. Am. Chem. Soc.* 131 (2009) 177.
- [20] K. Striebel, F. McLarnon, E. Cairns, *J. Electrochem. Soc.* 137 (1990) 3351.
- [21] W. Hayduk, H. Laudie, *AIChE J.* 20 (1974) 611.
- [22] D. Tromans, *Hydrometallurgy* 50 (1998) 279.
- [23] R. Kjellander, J. Ulander, *Mol. Phys.* 95 (1998) 495.
- [24] A. Damjanovic, M. Genshaw, J. Bockris, *J. Electroanal. Chem.* 15 (1967) 173.
- [25] L. Jiang, A. Hsu, D. Chu, R. Chen, *J. Electrochem. Soc.* 156 (2009) B370.
- [26] J. Prakash, H. Joachin, *Electrochim. Acta* 42 (2000) 2289.
- [27] L. Adams, S. Poynton, C. Tamain, R. Slade, J. Varcoe, *Chem. Sust. Chem.* 1 (2008) 79.
- [28] J. Zhou, M. Unlu, J. Vega, P. Kohl, *J. Power Sources* 190 (2009) 285.
- [29] C. Lang, K. Kim, P. Kohl, *Electrochem. Solid State* 9 (2006) A545.